

A Unified Approach to Predict Near and Far-Field Acoustic Pressures from Lighthill's Analogy

P. Croaker¹, N. Kessissoglou¹, S. Marburg²

¹ School of Mechanical and Manufacturing Engineering
 The University of New South Wales, Sydney, NSW 2052, Australia

² LRT4 – Institute of Mechanics
 Universität der Bundeswehr München, D-85579 Neubiberg, Germany

Abstract

A unified approach to predict near and far-field acoustic pressures based on Lighthill's acoustic analogy is presented. Numerical techniques are implemented to remove the singularities that occur when the integral form of Lighthill's acoustic analogy is applied in the near-field. As the distance between the source and field point increases, the approach presented here behaves as a standard far-field implementation of Lighthill's analogy. The accuracy of the method is demonstrated by computing the near-field acoustic pressures arising from an analytical acoustic source distribution and comparing the results with those obtained using an alternate formulation from the literature.

Introduction

Lighthill reformulated the Navier-Stokes equation into a wave equation that represents the acoustic source generation by fluid motion and the propagation of these acoustic sources [5, 6]. He derived an acoustic analogy which demonstrates that sound generated by a turbulent fluid flow is equivalent to the sound generated by a distribution of acoustic quadrupoles computed from the instantaneous velocity fluctuations.

A range of hybrid methods which use computational fluid dynamics (CFD) to calculate acoustic source terms from transient flow variables and Lighthill's acoustic analogy to predict the acoustic propagation have been developed [1, 7]. These hybrid methods typically make use of the Green's function solution of the wave equation to reformulate the acoustic propagation problem into an integral equation. Direct application of this approach to Lighthill's analogy results in an integral equation where the acoustic waves generated by the source distribution propagate to the far-field as monopoles. Any numerical errors present in the source field can thereby swamp the far-field response. In many hybrid methods, this monopolar integral equation is converted to a quadrupolar integral equation by applying the divergence theorem. The acoustic waves generated by this quadrupolar integral equation then propagate to the far-field as quadrupoles. This approach has been shown to produce accurate results and does not suffer from the error amplification experienced with the monopolar integral equation [1, 7].

Recently some attention has been given to using a quadrupole form of the integral equation to predict the acoustic pressure inside the source region [4, 10]. In the vicinity of the field point, the integrand is not continuous due to the singularity of the Green's function and its derivatives. Hence a small volume around the field point must be excluded from the domain before the divergence theorem can be applied. Singular and 'near-singular' volume integrals arise from this approach, as well as some extra terms due to the small exclusion volume. Whilst Watrigan [10] takes these extra terms into account, no treatment of the singular volume integrals is provided. Khalighi [4] also includes the extra terms due to the exclusion volume. The singular volume integrals are converted to singular surface integrals

using the divergence theorem and then solved using a singularity subtraction technique. Neither approach applies any specific treatment for the near-singular integrals.

In this paper, near-field formulations for both the monopole and quadrupole form of Lighthill's analogy are presented. The monopole formulation is developed for use as a reference solution. The quadrupole formulation is similar to those presented by Watrigan [10] and Khalighi [4]. In the present work, the singular volume integrals are regularised using the singularity subtraction technique of Guiggiani et al. [2, 3] and the near-singular volume integrals are treated using the self-adaptive polynomial transformation technique of Telles [8, 9]. Both the monopole and quadrupole formulations are applied to predict the near-field acoustic pressure generated by a distribution of Lighthill's tensor that has an analytical spatial variation. The results from both formulations are compared.

Numerical Methods

Monopole Formulation of Lighthill's Analogy

An integral equation for calculating the acoustic pressure, p_a , at a field point, \mathbf{x} , based on Lighthill's analogy can be expressed as [5, 7]

$$\hat{p}_a(\mathbf{x}, \omega) = \int_{\Omega} \frac{\partial^2 \hat{T}_{ij}(\mathbf{y}, \omega)}{\partial y_i \partial y_j} \hat{G}_k(\mathbf{x}, \mathbf{y}) dy \quad (1)$$

where a harmonic time dependence of $e^{-i\omega t}$ has been assumed. u_i and u_j are the i^{th} and j^{th} components of the velocity vector, respectively. $\hat{G}_k(\mathbf{x}, \mathbf{y}) = \frac{e^{ikr}}{4\pi r}$ is the harmonic free-field Green's function, k is the acoustic wavenumber, \mathbf{y} is the source point and $r = |\mathbf{x} - \mathbf{y}|$. p_a is the acoustic pressure and T_{ij} is the Lighthill tensor. For low Mach number flows, T_{ij} can be expressed as [5]

$$T_{ij} \approx \rho_0 u_i u_j \quad (2)$$

where ρ_0 is the incompressible density. In equation (1), \hat{T}_{ij} and \hat{p}_a represent the Fourier transforms of T_{ij} and p_a , respectively.

For the present work, it is assumed that a region of space, Ω , with boundary, Γ , contains a spatially varying distribution of Lighthill's tensor. Outside this boundary, Γ , Lighthill's tensor is zero. In the current work, the boundary is not hard walled and acoustic waves pass unhindered through the boundary. Furthermore, it is assumed that no field point lies on or near the boundary and hence evaluation of singular and 'near-singular' surface integrals is not considered. Hence this work focuses on singular and near-singular volume integrals only.

The formulation given by equation (1) is only valid when the field point is outside the acoustic source region. When the field point is inside the acoustic source region, the integral contains a singularity and cannot be solved directly. To overcome this, a small spherical volume, V_ϵ , of radius ϵ and bounded by the surface ∂V_ϵ , is taken around the field point and equation (1) is

rewritten as

$$\hat{p}_a(\mathbf{x}, \omega) = \lim_{\varepsilon \rightarrow 0} \int_{(\Omega - V_\varepsilon)} \frac{\partial^2 \hat{T}_{ij}(\mathbf{y}, \omega)}{\partial y_i \partial y_j} \hat{G}_k(\mathbf{x}, \mathbf{y}) d\mathbf{y} + \lim_{\varepsilon \rightarrow 0} \int_{V_\varepsilon} \frac{\partial^2 \hat{T}_{ij}(\mathbf{y}, \omega)}{\partial y_i \partial y_j} \hat{G}_k(\mathbf{x}, \mathbf{y}) d\mathbf{y} \quad (3)$$

Watrigan [10] demonstrated that the second term on the right hand side of equation (3) is zero and hence equation (3) reduces to

$$\hat{p}_a(\mathbf{x}, \omega) = \lim_{\varepsilon \rightarrow 0} \int_{(\Omega - V_\varepsilon)} \frac{\partial^2 \hat{T}_{ij}(\mathbf{y}, \omega)}{\partial y_i \partial y_j} \hat{G}_k(\mathbf{x}, \mathbf{y}) d\mathbf{y} \quad (4)$$

Equation (4) will be referred to as the ‘monopole formulation’ of Lighthill’s analogy, as the acoustic sources given by $\frac{\partial^2 \hat{T}_{ij}}{\partial y_i \partial y_j}$ produce acoustic waves which propagate away from the source point, \mathbf{y} , as monopoles. However, errors in the acoustic source distribution also radiate to the far-field as monopoles. Any such errors can produce inaccurate acoustic pressure predictions. Hence, the monopole formulation is not suitable for use in the far-field. The monopole formulation is used here to validate the near-field pressures predicted with the quadrupole formulation.

Quadrupole Formulation of Lighthill’s Analogy

An alternate formulation to equation (1) commonly used for far-field noise predictions based on Lighthill’s analogy is given by [7]

$$\hat{p}_a(\mathbf{x}, \omega) = \int_{\Omega} \hat{T}_{ij}(\mathbf{y}, \omega) \frac{\partial^2 \hat{G}_k(\mathbf{x}, \mathbf{y})}{\partial y_i \partial y_j} d\mathbf{y} \quad (5)$$

This formulation relies on applying the divergence theorem to equation (1) to move the spatial derivatives from Lighthill’s stress tensor to the Green’s function. However, when the field point is inside the source region, the divergence theorem must be applied to equation (3) instead, producing

$$\begin{aligned} \hat{p}_a(\mathbf{x}, \omega) &= \lim_{\varepsilon \rightarrow 0} \int_{(\Omega - V_\varepsilon)} \hat{T}_{ij}(\mathbf{y}, \omega) \frac{\partial^2 \hat{G}_k(\mathbf{x}, \mathbf{y})}{\partial y_i \partial y_j} d\mathbf{y} \\ &+ \lim_{\varepsilon \rightarrow 0} \int_{V_\varepsilon} \frac{\partial^2 \hat{T}_{ij}(\mathbf{y}, \omega)}{\partial y_i \partial y_j} \hat{G}_k(\mathbf{x}, \mathbf{y}) d\mathbf{y} \\ &+ \lim_{\varepsilon \rightarrow 0} \int_{\partial V_\varepsilon} \left[\hat{G}_k(\mathbf{x}, \mathbf{y}) \frac{\partial \hat{T}_{ij}(\mathbf{y}, \omega)}{\partial y_i} \cdot n_j - \hat{T}_{ij} \frac{\partial \hat{G}_k(\mathbf{x}, \mathbf{y})}{\partial y_j} \cdot n_i \right] d\mathbf{y} \\ &+ \int_{\Gamma} \left[\hat{G}_k(\mathbf{x}, \mathbf{y}) \frac{\partial \hat{T}_{ij}(\mathbf{y}, \omega)}{\partial y_i} \cdot n_j - \hat{T}_{ij} \frac{\partial \hat{G}_k(\mathbf{x}, \mathbf{y})}{\partial y_j} \cdot n_i \right] d\mathbf{y} \quad (6) \end{aligned}$$

where n_i is the i^{th} component of the normal vector pointing out of the fluid on ∂V_ε and Γ . Using results from Watrigan [10], equation (6) can be expressed as

$$\begin{aligned} \hat{p}_a(\mathbf{x}, \omega) &= \lim_{\varepsilon \rightarrow 0} \int_{(\Omega - V_\varepsilon)} \hat{T}_{ij}(\mathbf{y}, \omega) \frac{\partial^2 \hat{G}_k(\mathbf{x}, \mathbf{y})}{\partial y_i \partial y_j} d\mathbf{y} - \frac{\sum_{i=1}^d T_{ii}(\mathbf{x}, \omega)}{d} \\ &+ \int_{\Gamma} \left[\hat{G}_k(\mathbf{x}, \mathbf{y}) \frac{\partial \hat{T}_{ij}(\mathbf{y}, \omega)}{\partial y_i} \cdot n_j - \hat{T}_{ij} \frac{\partial \hat{G}_k(\mathbf{x}, \mathbf{y})}{\partial y_j} \cdot n_i \right] d\mathbf{y} \quad (7) \end{aligned}$$

where d is the dimension of the problem. Equation (7) here is referred to as the ‘quadrupole formulation’ of Lighthill’s analogy.

Finite Element Discretisation

The source region is initially discretised into finite elements and partitioned into two regions: Ω_s , representing the finite elements that intersect with the vanishing neighbourhood, and Ω_o , representing the finite elements that do not intersect with the vanishing neighbourhood. Also, the boundary of the source region, Γ , is discretised into finite elements, Γ_0 . Hexahedral elements are used for the source region and quadrilateral elements are used for the boundary. All elements are mapped onto a reference element in intrinsic coordinates. For the volume elements, the

intrinsic coordinates are denoted by $\boldsymbol{\xi} = (\xi, \eta, \zeta)$ and for the surface elements they are $\boldsymbol{\psi} = (\psi, \kappa)$. In the present work, a trilinear mapping is used for the volume elements and a bilinear mapping for the surface elements, which allows the value of any variable within the element to be calculated as follows

$$\alpha_v(\boldsymbol{\xi}) = \sum_m M_v^m(\boldsymbol{\xi}) \alpha_v^m, \quad \alpha_s(\boldsymbol{\psi}) = \sum_m M_s^m(\boldsymbol{\psi}) \alpha_s^m \quad (8)$$

where α_v represents any variable in the volume and α_s represents any variable on the surface. m represents the nodes used to define the geometry. $M_v^m(\boldsymbol{\xi})$ and $M_s^m(\boldsymbol{\psi})$ are the shape functions of the geometry for the volume and surface elements, respectively. \mathbf{y}^m are the Cartesian coordinates of the m^{th} node.

During the mapping process, each element in Ω_s is mapped onto a reference cube, Ω_{SR} , in intrinsic coordinates. Similarly, the exclusion neighbourhood is mapped from a region, V_ε , in Cartesian coordinates to a region, σ_ε , in intrinsic coordinates. Also, elements in region Ω_0 map onto a region Ω_{OR} , in intrinsic coordinates.

In intrinsic coordinates, equation (4) can be expressed as

$$\begin{aligned} \hat{p}_a(\mathbf{x}, \omega) &= \lim_{\varepsilon \rightarrow 0} \int_{(\Omega_{SR} - \sigma_\varepsilon)} \frac{\partial^2 \hat{T}_{ij}}{\partial y_i \partial y_j}(\mathbf{y}(\boldsymbol{\xi}), \omega) \hat{G}_k(\mathbf{x}, \mathbf{y}(\boldsymbol{\xi})) J(\boldsymbol{\xi}) d\xi d\eta d\zeta \\ &+ \int_{\Omega_{OR}} \frac{\partial^2 \hat{T}_{ij}}{\partial y_i \partial y_j}(\mathbf{y}(\boldsymbol{\xi}), \omega) \hat{G}_k(\mathbf{x}, \mathbf{y}(\boldsymbol{\xi})) J(\boldsymbol{\xi}) d\xi d\eta d\zeta \quad (9) \end{aligned}$$

and equation (7) can be expressed as

$$\begin{aligned} \hat{p}_a(\mathbf{x}, \omega) &= \lim_{\varepsilon \rightarrow 0} \int_{(\Omega_{SR} - \sigma_\varepsilon)} \hat{T}_{ij}(\mathbf{y}(\boldsymbol{\xi}), \omega) \frac{\partial^2 \hat{G}_k(\mathbf{x}, \mathbf{y}(\boldsymbol{\xi}))}{\partial y_i \partial y_j} J(\boldsymbol{\xi}) d\xi d\eta d\zeta \\ &+ \int_{\Omega_{OR}} \hat{T}_{ij}(\mathbf{y}(\boldsymbol{\xi}), \omega) \frac{\partial^2 \hat{G}_k(\mathbf{x}, \mathbf{y}(\boldsymbol{\xi}))}{\partial y_i \partial y_j} J(\boldsymbol{\xi}) d\xi d\eta d\zeta \\ &- \frac{\sum_{i=1}^d T_{ii}(\mathbf{x}, \omega)}{d} + \int_{\Gamma_0} \left[\hat{G}_k(\mathbf{x}, \mathbf{y}(\boldsymbol{\xi})) \frac{\partial \hat{T}_{ij}(\mathbf{y}(\boldsymbol{\xi}), \omega)}{\partial y_i} \cdot n_j \right. \\ &\left. - \hat{T}_{ij} \frac{\partial \hat{G}_k(\mathbf{x}, \mathbf{y}(\boldsymbol{\xi}))}{\partial y_j} \cdot n_i \right] J(\boldsymbol{\psi}) d\psi d\kappa \quad (10) \end{aligned}$$

where $J(\boldsymbol{\xi})$ and $J(\boldsymbol{\psi})$ are the Jacobian of the transformations from Cartesian to intrinsic coordinates for volume element and surface elements, respectively.

Regularisation of Singular Integrals

The first terms on the right hand side of equations (9) and (10) are singular and cannot be evaluated by standard numerical integration. To remove these singularities, a coordinate transformation to spherical coordinates, $\boldsymbol{\rho} = (\rho, \theta, \phi)$, is employed. These spherical coordinates are centred at $\boldsymbol{\xi}_0 = (\xi_0, \eta_0, \zeta_0)$, the image of \mathbf{x} in intrinsic coordinates, and are given by

$$\xi = \xi_0 + \rho \cos \theta \sin \phi, \quad \eta = \eta_0 + \rho \sin \theta \sin \phi, \quad \zeta = \zeta_0 + \rho \cos \phi \quad (11)$$

where ρ is the radius, θ is the azimuth angle and ϕ is the zenith angle. The Jacobian of the transformation from intrinsic to spherical coordinates results in the following relationship

$$d\xi d\eta d\zeta = \rho^2 \sin \phi d\rho d\theta d\phi \quad (12)$$

This spherical coordinate transformation is sufficient to regularise the singularity in equation (9) and the monopole formulation can then be solved using standard quadrature techniques. Transformation to spherical coordinates weakens the singularity of equation (10) to $O(\rho^{-1})$. To regularise the remaining singularity, the singularity subtraction technique of Guiggiani et al. [2, 3] is used. After application of Guiggiani’s regularisation technique [2, 3], the singular integrals of equation (10) can be calculated accurately using Gaussian quadrature.

Treatment of Near-Singular Integrals

Near-singular integrals are regular integrals and can hence be solved numerically using standard quadrature schemes. However, when the field point is located close to an element, the number of integration points required to achieve an accurate solution becomes large. Coordinate transformation techniques cluster the integration points towards the singularity. Using a self-adaptive polynomial transformation technique [8, 9], this integration point clustering is related to the distance between field point and element. Hence, as the distance increases, the distribution of integration points within the element reverts to normal. This allows the technique to be easily applied to all near-singular integrals within the model.

Results and Discussions

Analytical Source

The source region used in the current study is a 1m cube that is centred at the origin. Analytical velocity distributions are assigned inside the cube as follows

$$\hat{u}_i = \frac{A_i}{2\omega} e^{ik_i y_i} \quad (13)$$

where A_i is a constant, $\omega = kc$ is the radian frequency with c the speed of sound. k_i is the wavenumber of the i^{th} component of velocity. This produces the following distribution of Lighthill's tensor within the cube

$$\hat{T}_{ij} = \frac{A_i A_j}{4\omega^2} e^{j(k_i y_i + k_j y_j)} \quad (14)$$

The single and double spatial derivatives of Lighthill's tensor are

$$\begin{aligned} \frac{\partial \hat{T}_{ij}}{\partial y_i} &= \frac{ik_i A_i A_j}{4\omega^2} e^{j(k_i y_i + k_j y_j)} \\ \frac{\partial^2 \hat{T}_{ij}}{\partial y_i \partial y_j} &= -\frac{k_i k_j A_i A_j}{4\omega^2} e^{j(k_i y_i + k_j y_j)} \end{aligned} \quad (15)$$

It is relatively straightforward to determine the nodal values of Lighthill's tensor and its single and double spatial derivatives. This makes the analytical source distribution an ideal choice for comparing the monopole and quadrupole formulations. A similar approach was used by Watrigant [10].

Three analysis cases were studied. Table 1 summarises the parameters used for the comparative studies. The speed of sound for all studies was $c = 1500\text{m/s}$ and the frequency, $f = \frac{\omega}{2\pi}$. For each analysis case three different element sizes were studied. The number of nodes in each coordinate direction was 70, 140 and 280, resulting in element edge lengths of $\Delta l = 1.45\text{E}-02$, $7.19\text{E}-03$ and $3.58\text{E}-03$, respectively.

Table 1: Parameters for the comparative analyses

Parameter	Units	Case 1	Case 2	Case 3
k	m^{-1}	2π	0.2π	0.02π
f	Hz	$1.5\text{E}+03$	$1.5\text{E}+02$	$1.5\text{E}+01$
A_1	-	$2.0\text{E}+03$	$2.0\text{E}+03$	$2.0\text{E}+03$
k_1	m^{-1}	2π	2π	2π
A_2	-	$5.0\text{E}+02$	$5.0\text{E}+02$	$5.0\text{E}+02$
k_2	m^{-1}	4π	4π	4π
A_3	-	$1.0\text{E}+03$	$1.0\text{E}+03$	$1.0\text{E}+03$
k_3	m^{-1}	8π	8π	8π

Figure 1 shows the magnitude and phase of the double spatial derivative of Lighthill's tensor, $\frac{\partial^2 \hat{T}_{ij}}{\partial y_i \partial y_j}$, inside the source region for the parameters given in Table 1.

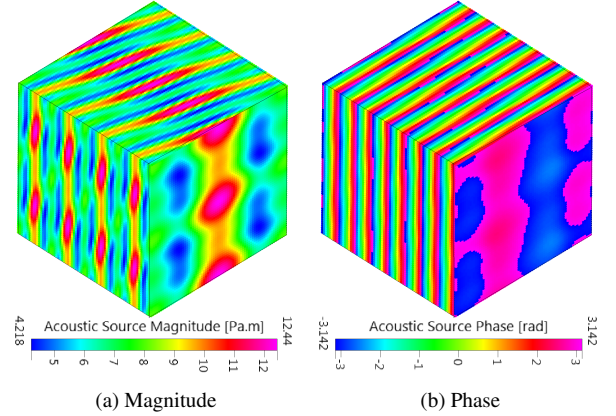


Figure 1: Spatial distribution of the double spatial derivative of Lighthill's tensor

Near-Field Acoustic Pressures

To assess the accuracy of the quadrupole formulation, the acoustic pressure was recovered within the source region at field points ranging from $(-0.4, 0, 0)$ to $(0.4, 0, 0)$ in $(0.008, 0, 0)$ increments. Figure 2 shows the real and imaginary components of the acoustic pressure for the three cases studied. For clarity, only the pressures obtained using the monopole formulation with the finest grid resolution are presented. Figure 2 shows that the near-field acoustic pressures for the $k = 0.2\pi$ and $k = 0.02\pi$ cases have similar profiles and this is likely due to the compactness of the acoustic source region at these wavenumbers.

To estimate the accuracy of the quadrupole formulations, the following two error metrics were defined:

$$E(\mathbf{x}) = \frac{|p_{aq}(\mathbf{x}) - p_{am}(\mathbf{x})|}{|p_{am}(\mathbf{x})|}, \quad E_{av} = \frac{\|p_{aq}(\mathbf{x}) - p_{am}(\mathbf{x})\|_2}{\|p_{am}(\mathbf{x})\|_2} \quad (16)$$

where $\|\cdot\|_2$ represents the L2-norm, $E(\mathbf{x})$ is the relative error at the field point, \mathbf{x} , and E_{av} is the average relative error. $p_{aq}(\mathbf{x})$ refers to the acoustic pressure predicted using the quadrupole formulation and $p_{am}(\mathbf{x})$ is the acoustic pressure predicted using the monopole formulation. Figure 3 shows the local relative error at each wavenumber for the three grid resolutions considered. In all plots the local relative error has small oscillations caused by variations in the field point position relative to nearby element boundaries.

Table 2 provides a summary of E_{av} for the quadrupole formulation relative to the monopole formulation. The quadrupole formulation predicts the near-field acoustic pressure with good accuracy over a wide range of wavenumbers and grid spacing.

Table 2: Summary of average error of quadrupole formulation

Δl	$k = 2\pi$	$k = 0.2\pi$	$k = 0.02\pi$
$1.45\text{E}-02$	$2.9\text{E}-03$	$7.2\text{E}-03$	$7.2\text{E}-03$
$7.19\text{E}-03$	$7.2\text{E}-04$	$1.8\text{E}-03$	$1.8\text{E}-03$
$3.58\text{E}-03$	$1.8\text{E}-04$	$4.5\text{E}-04$	$4.5\text{E}-04$

Conclusions

A near-field quadrupole formulation of Lighthill's analogy has been presented and the results compared with a monopole formulation. The quadrupole formulation relies on a singularity subtraction technique to solve the singular volume integrals and on a self-adaptive polynomial transformation to solve the near-singular integrals. The quadrupole formulation was applied to

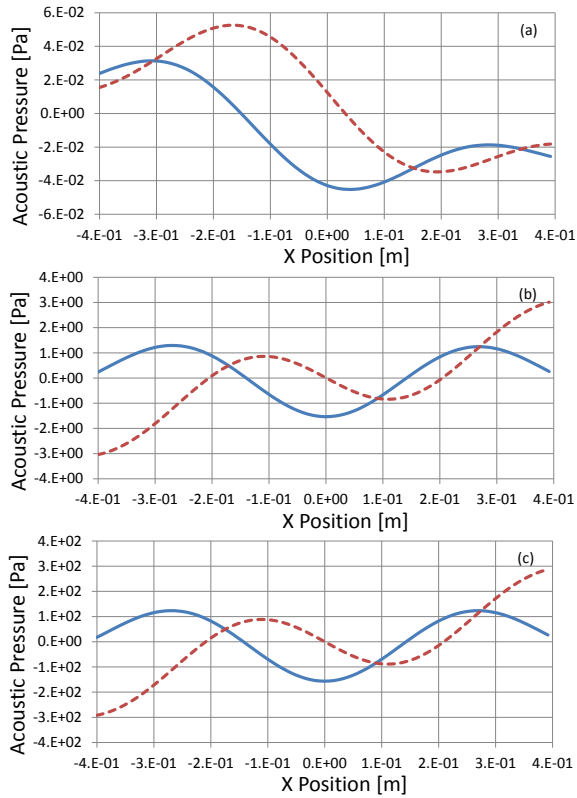


Figure 2: Real (solid) and imaginary (dashed) acoustic pressures for wavenumbers (a) $k = 2\pi$, (b) $k = 0.2\pi$ and (c) $k = 0.02\pi$

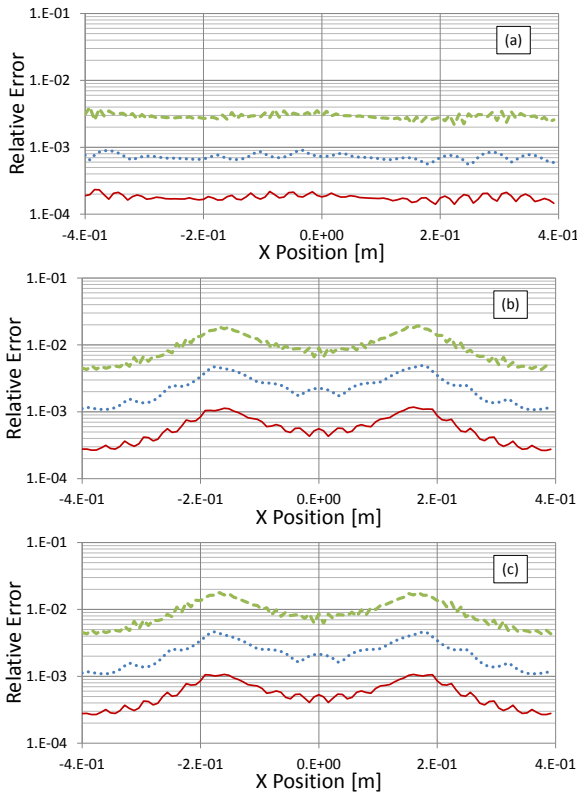


Figure 3: Local error of quadrupole formulation for $\Delta t = 1.45E-02$ (dashed), $7.19E-03$ (dotted) and $3.58E-03$ (solid) for wavenumbers (a) $k = 2\pi$, (b) $k = 0.2\pi$ and (c) $k = 0.02\pi$

predict the near-field pressures generated by an acoustic source distribution described by an analytical spatial variation. The quadrupole formulation predicts the near-field acoustic pressure with good accuracy over a wide range of wavenumbers. The average error, relative to the results from the monopole formulation, did not exceed 0.8% for all of the cases considered.

Acknowledgements

Funding for this work has been provided by the Maritime Platforms Division of the Defence Science and Technology Organisation.

References

- [1] Gloerfelt, X., Pérot, F., Bailly, C. and Juvé, D., Flow-induced cylinder noise formulated as a diffraction problem for low Mach numbers, *Journal of Sound and Vibration*, **287**, 2005, 129–151.
- [2] Guiggiani, M. and Gigante, A., A general algorithm for multidimensional Cauchy principal value integrals in the boundary element method, *ASME Journal of Applied Mechanics*, **57**, 1990, 906–915.
- [3] Guiggiani, M., Krishnasamy, G., Rudolph, T. J. and Rizzo, F. J., A general algorithm for the numerical solution of hypersingular boundary integral equations, *ASME Journal of Applied Mechanics*, **59**, 1992, 604–614.
- [4] Khalighi, Y., *Computational Aeroacoustics of Complex Flows at Low Mach Number*, Ph.D. Thesis, Stanford University, 2010.
- [5] Lighthill, M. J., On sound generated aerodynamically, I. General theory, *Proceedings of the Royal Society A*, **211**, 1952, 564–587.
- [6] Lighthill, M. J., On sound generated aerodynamically, II. Turbulence as a source of sound, *Proceedings of the Royal Society A*, **222**, 1954, 1–32.
- [7] Martínez-Lera, P. and Schram, C., Correction techniques for the truncation of the source field in acoustic analogies, *Journal of the Acoustical Society of America*, **124**, 2008, 3421–3429.
- [8] Telles, J. C. F., A self-adaptive co-ordinate transformation for efficient numerical evaluation of general boundary element integrals, *International Journal for Numerical Methods in Engineering*, **24**, 1987, 959–973.
- [9] Telles, J. C. F. and Oliveira, R. F., Third degree polynomial transformation for boundary element integrals: Further improvements, *Engineering Analysis with Boundary Elements*, **13**, 1994, 135–141.
- [10] Watrigant, M., *Investigation des Méthodes D'Estimation en Aéroacoustique Automobile par Résolution Temporelle Rapide des Équations Intégrales*, Ph.D. Thesis, École Supérieure d'Ingénieurs de Poitiers, 2010.